crystals

MDPI

Article

Influence of Chloride Ion Concentration on Corrosion Behavior of WC–MgO Composite

Bowen Fan [1,2], Tao Qin [1,*], Ying Zhang [1] and Jinyi Wang [1]

[1] School of Mechanical Engineering, Wuxi Institute of Technology, Wuxi 214121, China; fanbw@wxit.edu.cn (B.F.); zhangying@wxit.edu.cn (Y.Z.); wangjy@wxit.edu.cn (J.W.)
[2] College of Mechanical Engineering, Donghua University, Shanghai 201620, China
* Correspondence: qint@wxit.edu.cn

Abstract: The influence of chloride ion (Cl^-) concentration on the corrosion mechanism of WC–MgO composites has been studied in this work. The results suggest that the corrosion resistance of WC–MgO composite decreases first and then increases with the increase in Cl^- concentration. Solution conductivity and dissolved oxygen content are the main influence factors. The solution conductivity determines the charge transfer process, and the dissolved oxygen determines the cathodic oxygen absorption reaction. The corrosion characteristic is typical pitting corrosion. Meanwhile, the corrosion mechanism contains an oxidation process of the WC matrix and the dissolution destruction of the MgO toughening phase. The formation of the WO_3 corrosion layer hinders the general corrosion to protect the inner material. However, the dissolution of MgO induces the initiation of pitting. The local alkaline caused by MgO dissolution promotes the dissolution of the WC matrix, which leads to the expansion of pitting.

Keywords: WC–MgO composite; chloride ion concentration; corrosion mechanism; pitting corrosion

Citation: Fan, B.; Qin, T.; Zhang, Y.; Wang, J. Influence of Chloride Ion Concentration on Corrosion Behavior of WC–MgO Composite. *Crystals* **2024**, *14*, 427. https://doi.org/10.3390/cryst14050427

Academic Editor: Shouxun Ji

Received: 8 April 2024
Revised: 25 April 2024
Accepted: 28 April 2024
Published: 30 April 2024

1. Introduction

WC–Co cemented carbide has been widely used as a cutting tool in the oil drilling and aerospace fields. It is composed of a WC matrix and a Co metal binder [1–3]. Its great mechanical properties depend on the good wettability of the Co binder with the WC hard phase. However, the Co binder is detrimental to the hardness and wear resistance of WC–Co cemented carbide [4,5]. Meanwhile, the consumption of Co is also increasing with the development of new energy industries [6]. Hence, there are some efforts to prepare new hard materials without or with little Co binder. Recently, cBN [7], ZrO_2 [8], Al_2O_3 [9], and MgO [10] have been used to prepared binderless WC cemented carbide.

For binderless cemented carbide, the mechanical property is the first concern, because it is the primary guarantee for engineering application and security. An aggressive environment is inevitable for cemented carbide [11]. Mechanical damage always interacts with corrosion to promote the early failure of cemented carbide. Hence, the corrosion resistance of cemented carbide is another important factor for engineering reliability. The mechanical properties are significantly influenced by surface conditions. In particular, the strength of a brittle material decreases significantly if microcracks or defects appear on the surface. The interaction of mechanical damage with a corrosion attack includes the following two processes: (1) a corrosion attack that promotes the rapid growth of mechanical damage defects [12]; (2) local mechanical damage that can destroy the passive film and then promote corrosion process. Especially for strength, the local minor defects will lead to a rapid reduction in strength. Hence, the study of the corrosion behavior of the WC-based composite is an important and critical part of improving its service life and application.

Replacing or part replacing Co binder has become a practicable method to improve its corrosion resistance. Recently, AISI304 [13], high-entropy alloys (HEAs) [14], Al_2O_3 [15], and VC [16] have been studied as replacements of Co binder. The replacement of Co

binder with other metals does not completely eliminate galvanic corrosion. Hence, high performance binderless cemented carbide is considered another method to obtain great corrosion resistance. Tang et al. [17] indicated that binderless WC hard material possesses better corrosion resistance compared with traditional WC–Co cemented carbide. Wang et al. [18] indicated that the corrosion resistance of a binderless WC–Y_2O_3–SiC_w composite in a H_2SO_4 solution was better than in a NaOH solution, which could be attributed to the formation of WO_3 film. Han et al. [19] studied the influence of a TiC addition on the corrosion behavior of a binderless WC–Al_2O_3 composite in an alkaline solution. Their result showed that the grain refinement and the formation of a TiO_2 oxide film were the main reasons for the increase in corrosion resistance.

WC–MgO composite has been prepared by hot-pressing sintering, which is considered to have the potential to replace WC–Co cemented carbide [10,20–23]. Because MgO is cheap and easy to obtain, the WC–MgO composite possesses broad application prospects for the replacement of WC–Co. Based on previous research [10], it has been proved that the WC–MgO composite possesses high hardness, fracture toughness, and moderate strength. The potential application contains special sealing for cooling water pumps or chemical equipment, high-pressure medium nozzles, etc. Previous researches also focus on improving mechanical properties, because mechanical performance is the foundation for ensuring its engineering applications. For the WC–MgO composite, however, the intrinsic brittleness makes it extremely sensitive to microcracks. Corrosion is one of the important forms of material failure, which is the main source of crack initiation. Hence, this study on corrosion behavior and the corrosion resistance of brittle WC–MgO composite has significant impact for application in the corrosion environment. In our previous works, the preliminary exploration of WC–MgO composite was conducted in acidic and alkaline environments [24]. The comparative study between WC–MgO composite and WC–Co cemented carbide was conducted in a NaCl solution [25]. However, the detailed corrosion mechanism has not been explored deeply. In particular, the initiation and propagation mechanism of pitting has not been clarified. Meanwhile, the relationship between NaCl solution concentration and passivation film has not yet been studied.

As we all know, chloride ion (Cl^-) is a kind of common strong activator that can destroy the passive film on the surface and promote pitting corrosion. Meanwhile, Cl^- possesses a small radius and a strong penetration ability. Hence, Cl^- can easily pass through the pores or defects in the passive film by diffusion or electric field action. Cl^- also shows strong adsorption capacity, and can adsorb and crowd out the adsorbed oxygen on the metal surface. The concentration of Cl^- depends on the corrosive environment of service conditions. Meanwhile corrosion is kind of performance-related to environmental systems. The adsorption process, conductivity, and material transfer characteristics are affected by the solution concentration. Hence, it is necessary to clarify the influence of Cl^- concentration on the corrosion mechanism of the WC–MgO composite.

In this work, the influence of Cl^- concentration on the corrosion behavior of WC–MgO composites was studied by soaking and electrochemical and microstructural analysis. The purpose of this study is to reveal the corrosion mechanism of WC–MgO composite in neutral NaCl solutions. Further, this study clarifies the intrinsic influencing factors of the corrosion behavior in different Cl^- concentration solutions. Based on this work, the corrosion control suggestions for WC–MgO composites are proposed.

2. Experiment Procedures

2.1. Material and Pretreatment

The material used in this work was prepared by hot-pressing sintering at 1650 °C for 90 min. The Vickers hardness and fracture toughness were 20.92 GPa and 9.85 MPa·$m^{1/2}$. The detailed composition can be seen in Ref [22]. Each sample was cut into 10 × 10 mm^2, which was also the exposed area of the working electrode. In order to conduct electrochemical experiments, all samples were encapsulated with epoxy resin. Meanwhile, copper wire

was used to ensure conductivity. To avoid the impact of surface defects on accuracy, 1 μm diamond paste was used to obtain the polishing surface.

2.2. Electrochemical Measurements

The NaCl powder used was guaranteed reagent (GR) sodium chloride produced by Sinopharm Chemical Reagent Co., Ltd. (Shanghai, China). The corrosion solution in this experiment was prepared with NaCl powder and distilled water. The concentration of the prepared NaCl solution was 0.1 wt.%, 1 wt.%, 3.5 wt.%, and 10 wt.%, wherein 3.5 wt.% NaCl solution was used to simulate the seawater environment.

The CS350H Electrochemical Workstation used in this work was produced by Wuhan Corrtest Instruments Corp., Ltd., Wuhan, China. All electrochemical tests were conducted at room temperature open to air. The standard three electrode system was used in this work, which contained a saturated calomel electrode (SCE), counter electrode (CE), and working electrode (WE). The counter electrode was composed of a platinum plate with an area of 10×10 mm^2. The open circuit potential, EIS, and polarization curves were conducted. The test duration of OCP was 4 h. For EIS measurement, the test potential was OCP with an amplitude perturbation voltage of 10 mV. The frequency scanning interval of EIS was from 10^{-3} to 10^6 Hz. The potential scanning interval of polarization curves was from -1 V to 1.5 V (vs. SCE reference electrode). In order to detect the influence of dissolved oxygen content in the solution, we set up a control group experiment. In that control group, high purity nitrogen (N_2) was continuously introduced into a 1 wt.% NaCl solution for 1 h to remove dissolved oxygen in the solution. To ensure the stability of the NaCl solution, the solution stood for 5 min before electrochemical measurements. During the process of electrochemical measurements, the introduction of high purity nitrogen (N_2) was stopped to avoid solution disturbance.

2.3. Microstructure and Composition Characterization

The phase structure was characterized by X-ray diffraction (XRD) using a D/max-2550PC (Rigaku Co., Ltd., Akishima, Japan) X-ray diffractometer with a Cu K-alpha radiation (λ = 0.154056 nm) at 40 kV and 20 mA. Scanning electron microscopy (SEM, Quanta 250, FEI Co., Hillsboro, OR, USA) and EDS were used to characterize the microstructure and element composition. Inductively coupled plasma atomic emission spectroscopy (ICP) was used to determine W and Mg element content in the NaCl solution after 60 days of soaking. The dissolved oxygen content in different concentrations of the NaCl solution was determined qualitatively by using the dissolved oxygen kit produced by Wuhu Jinghui Biotechnology Co., Ltd. (Wuhu, China). The color of the measured solution can clearly show the level of dissolved oxygen content. The darker color means higher dissolved oxygen content and the lighter color means lower dissolved oxygen content.

3. Results and Discussion

3.1. Electrochemical Corrosion Test

The OCP of the WC–MgO composite in the NaCl solution with different Cl^- concentration is presented in Figure 1. In the 0.1 wt.% NaCl solution, the OCP gradually shifts along the positive direction then becomes stable, showing no significant fluctuation. In the 1 wt.% NaCl solution, the OCP basically keeps stable during the immersion test. In the 3.5 wt.% NaCl solution, the OCP shifts along the positive direction first and then shifts along the negative direction. In the 10 wt.% NaCl solution, the OCP shifts along the negative direction. The result of the OCP indicates that the surface of the WC–MgO composite may be passivated in a low-concentration NaCl solution, which promotes OCP to shift along the positive direction. When the concentration of Cl^- is relatively high, the OCP shifts along the negative direction, which can be attributed to the destruction of the passivation film caused by Cl^-.

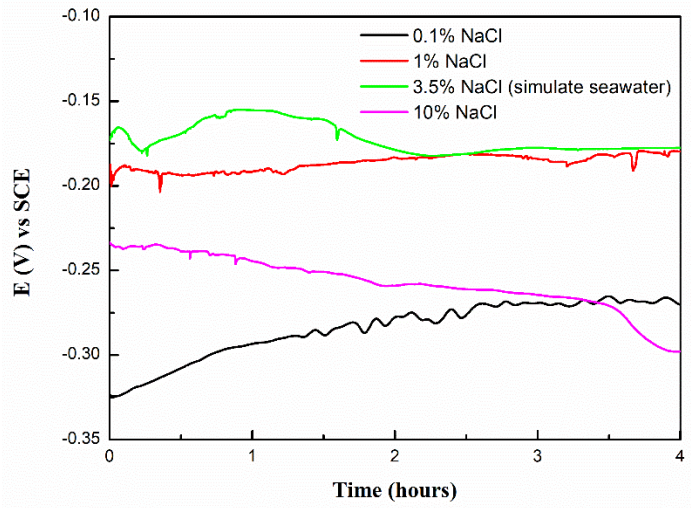

Figure 1. OCP of WC–MgO composite in NaCl solution with different Cl^- concentrations.

Through further comparison of stable OCP after 4 h of soaking, more negative OCP can be found in the 0.1 wt.% and 10 wt.% NaCl solutions. It is very clear that the corrosion tendency of the WC–MgO composite is nonlinear with the concentration of Cl^-, which may be attributed to the change of conductivity and dissolved oxygen of the NaCl solution. The change of solution conductivity directly affects the electron transfer process of electrochemical corrosion, while the change of dissolved oxygen affects the cathode oxygen absorption reaction. Meanwhile, Cl^- is a kind of highly adsorptive ion that can alter the electrochemical interface structure because of its adsorption on material surface. Hence, the influence of NaCl concentration on the electrochemical corrosion behavior of WC–MgO composites is extremely complicated.

The Tafel curves of WC–MgO composites in different concentrations of NaCl solution are presented in Figure 2a. The E_{corr} (corrosion potential) and I_{corr} (corrosion current density) fitting from the Tafel curve are shown in Figure 2b. As shown in Figure 2a, all the Tafel curves possess a similar shape. Meanwhile, the pseudo-passivation behavior can be found in the Tafel curves for WC–MgO composites in the NaCl solution. Pseudo-passivation behavior cannot effectively prevent the corrosion process. Similar pseudo-passivation behavior is also found in the $CoCrFeNiMo_{0.01}$ high-entropy alloy [26]. The passivation zone potential in the 1 wt.% NaCl solution is the most negative. It is clear that the current density of the passivation zone in the 1 wt.% NaCl solution is the highest, meaning it has the worst corrosion resistance.

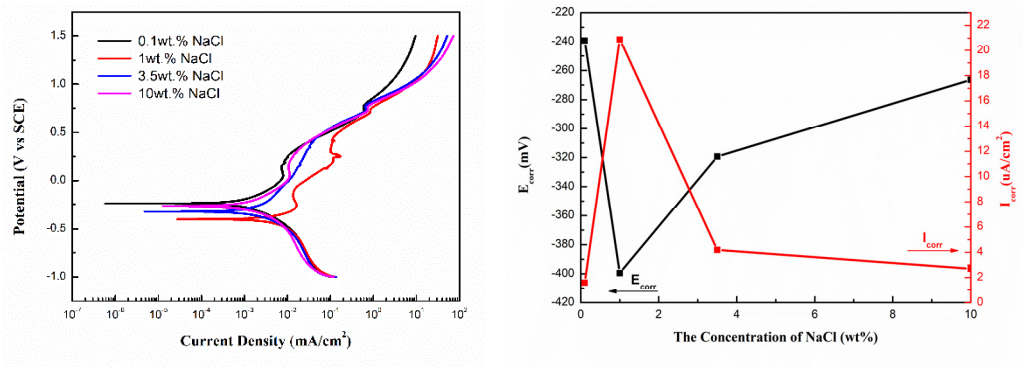

(**a**) (**b**)

Figure 2. Tafel curves (**a**) and E_{corr}/I_{corr} (**b**) of WC–MgO composite in NaCl solution with different Cl^- concentrations.

As shown in Figure 2b, the E_{corr} decreases and then increases with the increase in Cl^- concentration, while the I_{corr} increases and then decreases. The decrease in E_{corr} indicates a higher corrosion tendency. The increase in I_{corr} indicates a larger corrosion rate and worse corrosion resistance. In the 0.1 wt.% NaCl solution, the I_{corr} is lowest, at 1.59 uA/cm^2. As the Cl^- concentration increases to 1 wt.%, the I_{corr} significantly increases to 20.87 uA/cm^2. However, the I_{corr} decreases continuously as the Cl^- concentration further increases. The I_{corr} decreases to 2.7 uA/cm^2 when the Cl^- concentration reaches 10 wt.%. Hence, it is obvious that the WC–MgO composite possesses the largest I_{corr} quantity in the 1 wt.% NaCl solution, indicating the worst corrosion performance.

The EIS plots of WC–MgO composites in different concentration NaCl solutions are presented in Figure 3. According to the Nyquist plots in Figure 3a, similar analogous impedance characteristics can be found in all plots, meaning similar corrosion processes. The WC–MgO composite possesses the largest capacitive arcs in the 0.1 wt.% NaCl solution, and the lowest capacitive arcs in the 1 wt.% NaCl solution. The size of capacitive arcs describes the charge transfer resistance in the electrochemical reaction process, namely the resistance when the charge crosses the electrode interface. According to the Bode plots, the total impedance decreases from 220,104 Ohm.cm^2 to 40,370 Ohm.cm^2 as Cl^- concentration increases from 0.1 wt.% to 1 wt.%. Subsequently, the total impedance increases to 97,745 Ohm.cm^2 when the Cl^- concentration reaches 10 wt.%. The EIS result indicates that the corrosion resistance of the WC–MgO composite is lowest in the 1 wt.% NaCl solution, which is consistent with the Tafel curves results.

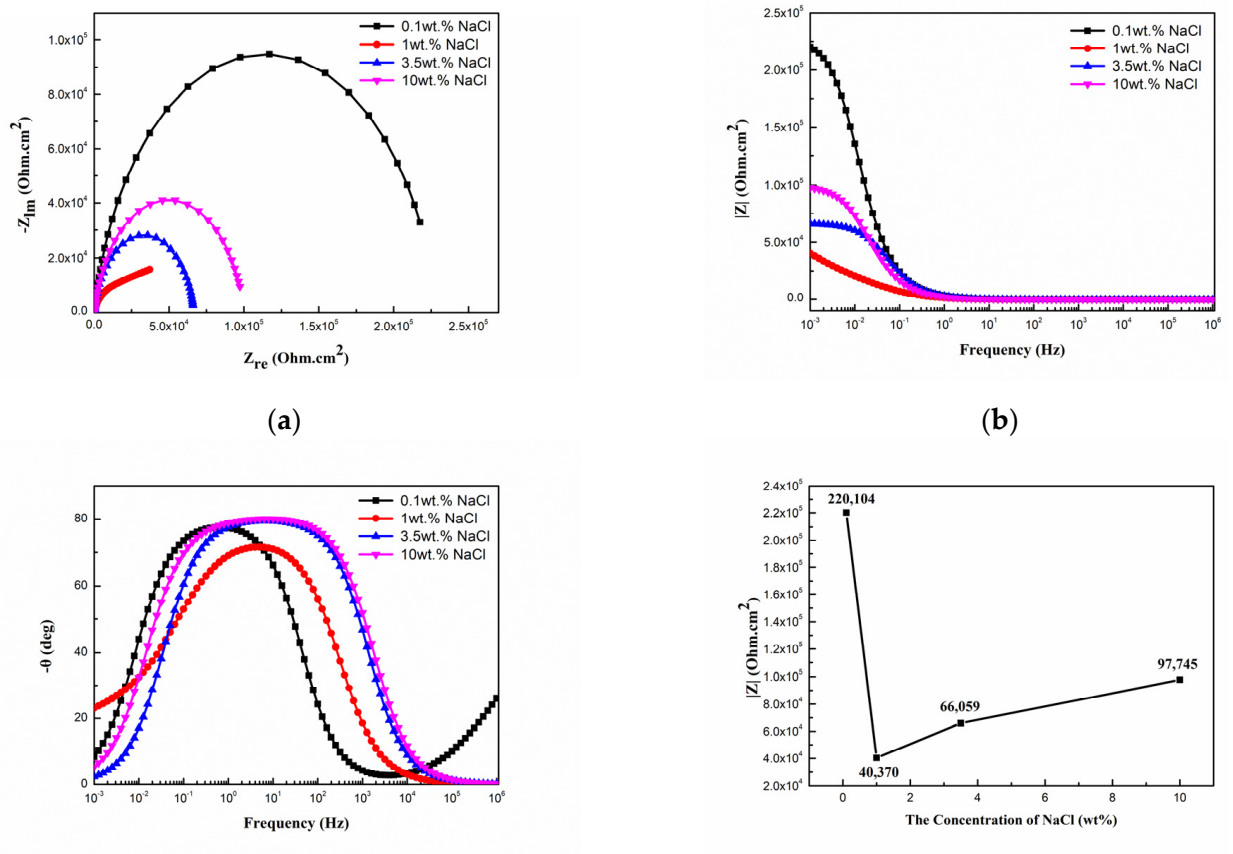

Figure 3. Nyquist (**a**), Bode (**b**,**c**) curves, and total impedance (**d**) of WC–MgO composite in NaCl solution with different Cl^- concentrations.

Raja et al. [27] pointed out that the electrode reaction process and passivation film formation process are both affected by dissolved oxygen. Obviously, dissolved oxygen

content will change with solution concentration. Hence, the dissolved oxygen content of the NaCl solution is determined qualitatively by using the dissolved oxygen kit. Meanwhile, the control group is set. In that control group, high purity nitrogen (N_2) is continuously introduced into the 1% NaCl solution for 1 h to remove dissolved oxygen before the electrochemical test. As shown in Figure 4, the darker color means a higher content of dissolved oxygen. It is clear that the content of dissolved oxygen decreases significantly with the increase in Cl^- concentration. Meanwhile, compared with the control group, the introduction of high purity nitrogen (N_2) promotes a significant decrease in the dissolved oxygen content in the 1 wt.% NaCl solution.

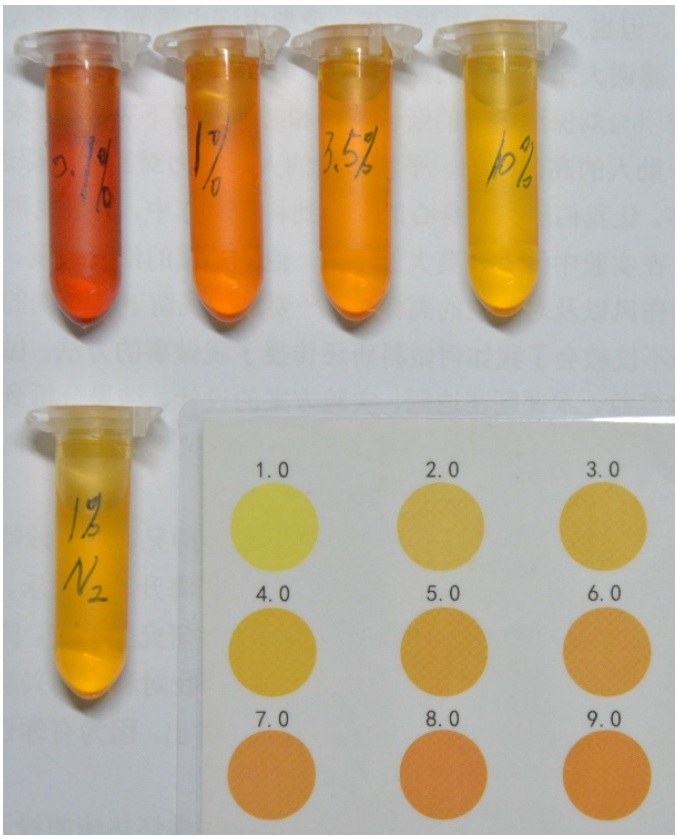

Figure 4. Dissolved oxygen content (mg/L) of NaCl solution with different Cl^- concentrations.

To explore the influence of the dissolved oxygen content on corrosion performance, the Tafel curves and EIS plots in the 1 wt.% NaCl solution and the control group are shown in Figure 5. As shown in Figure 5a, the current density decreases from 20.87 uA/cm^2 to 0.78 uA/cm^2 when the dissolved oxygen content decreases significantly. Meanwhile, the current density in the anodic polarization zone of the control group is also lower than the original group. It indicates that the decrease in the dissolved oxygen content inhibits the anodic dissolution rate and improves corrosion resistance in the NaCl solution. As shown in Figure 5b, the total impedance increases by 59.1% from 40,370 Ohm.cm^2 to 98,592 Ohm.cm^2 when the dissolved oxygen content decreases. It is widely known that the electrochemical corrosion mechanism includes an anodic process and a cathodic process. In the neutral solution, the cathodic process of electrochemical corrosion is generally the reduction of dissolved oxygen, namely the oxygen absorption reaction. Hence, the cathodic oxygen absorption reaction is an important factor affecting the corrosion process of the WC–MgO composite in the NaCl solution.

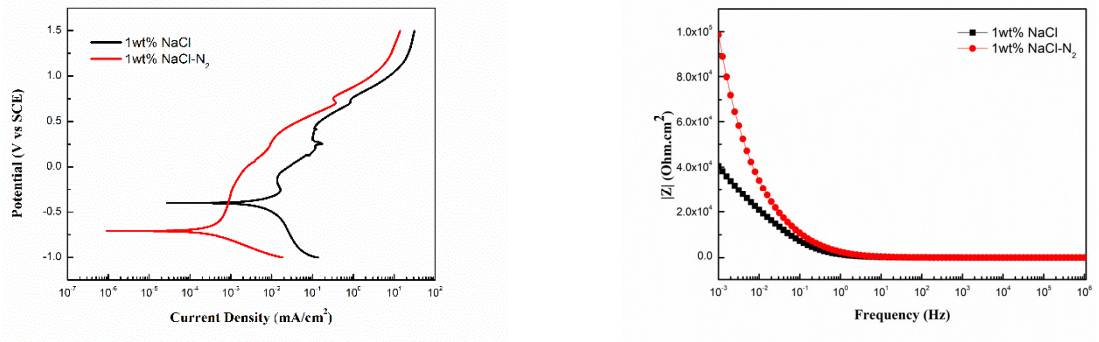

(**a**) (**b**)

Figure 5. Tafel (**a**) and impedance spectra (**b**) of WC–MgO composites in 1 wt.% NaCl solution with and without high purity nitrogen (N_2).

3.2. Characterization of the Corrosion Passivation Layer

The XRD, SEM, and mapping EDS are used to characterize corrosion products after the immersion corrosion test. Meanwhile, the ICP is also used to characterize the element content of the NaCl solution after soaking for 60 days.

As shown in Figure 6, the XRD patterns of the corroded and the origin sample are given. The main phase of the origin sample is WC. The MgO phase is not found due to its low content. Compared with the original sample, the WC phase peak intensity of the corroded surface is very low. Meanwhile, the WO_3 phase appears in the corroded surface of the WC–MgO composite. It is clear that WO_3 forms on the surface of the WC–MgO composite, which reduces the diffraction intensity of the WC matrix phase.

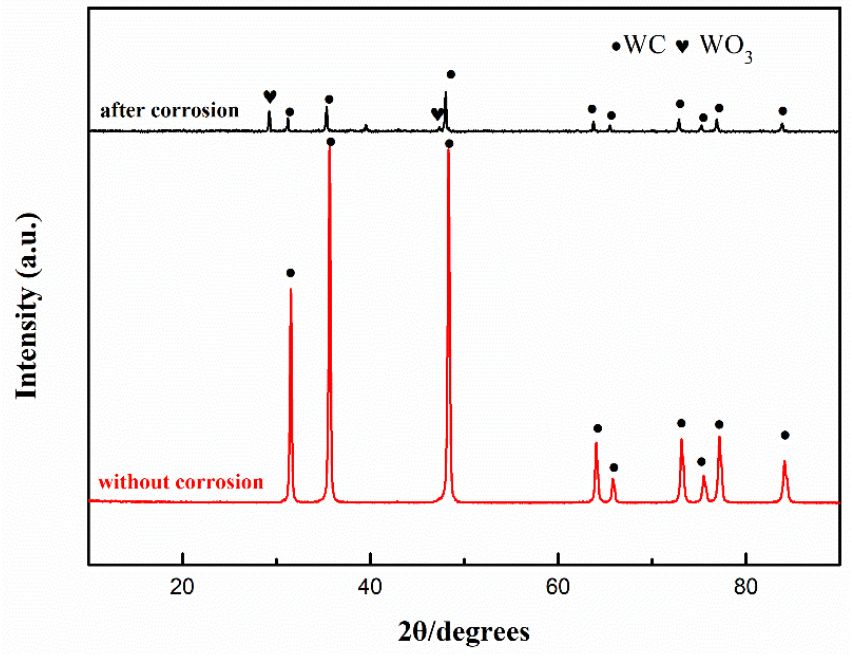

Figure 6. XRD patterns of WC–MgO composite with and without corrosion in 3.5 wt.%NaCl solution.

The SEM images of corrosion products in the 3.5 wt.%NaCl solution are given in Figure 7a,b, representing the surface and the cross-section of the corrosion layer, respectively. As shown in Figure 7a, the morphology of the corrosion products of the WC–MgO composite is relatively obvious and flat. It is also found that the corrosion products accumulate locally on the surface. As shown in Figure 7b, it is clear that the surface is completely and uniformly covered by the corrosion products. The thickness of the corrosion product layer is about 8–9 um.

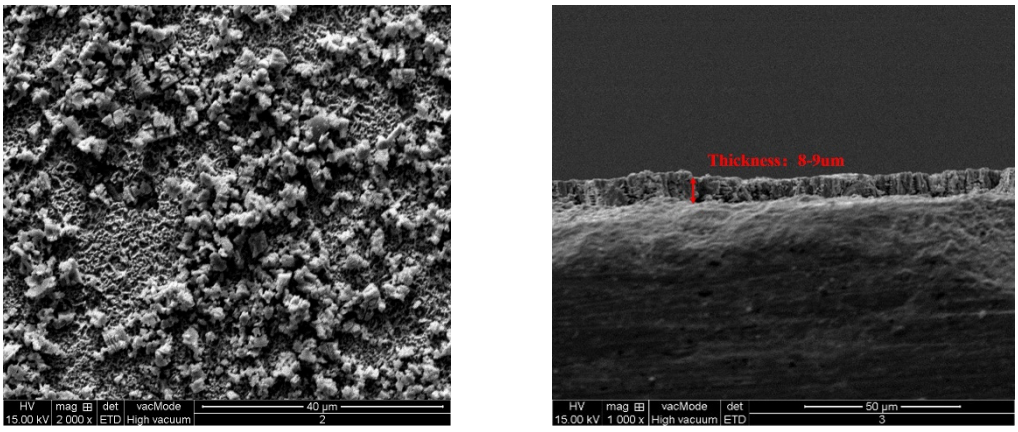

(**a**) (**b**)

Figure 7. SEM image of corrosion products of WC–MgO composites in 3.5 wt.% NaCl solution. Surface morphology after corrosion (**a**) and section morphology after corrosion (**b**).

Mapping EDS is used to characterize the chemical composition of the corrosion products, as shown in Figures 8 and 9. In the 1 wt.% NaCl solution, the main elements of the corrosion products contain tungsten (66.84 wt.%), carbon (8.88 wt.%), oxygen (21.46 wt.%), magnesium (1.23 wt.%), and sodium (1.59 wt.%). In the 3.5 wt.% NaCl solution, as shown in Figure 9, the main elements of the corrosion products contain tungsten (75.35 wt.%), carbon (15.62 wt.%), and oxygen (9.03 wt.%). It is found that the oxygen content of the corrosion products is relatively high in both the 1 wt.% and the 3.5 wt.% NaCl solutions. This indicates that the corrosion products are mainly composed of oxides. Compared with the 3.5 wt.% NaCl solution, cracks appear on the surface of the corrosion products in the 1 wt.% NaCl solution. Meanwhile, the sodium element is found in the corrosion products corroded in the 1 wt.% NaCl solution. This means that the corrosion products are loose, and the corrosion solution is easier to penetrate. It is difficult to completely clean the loose corrosion products from the NaCl solution, and they easily remain in the corrosion product. Hence, in the 1 wt.% NaCl solution, the corrosion products cannot protect the internal material from further corrosion, which is consistent with the worst corrosion resistance. Combined with the XRD results, it is inferred that the main corrosion product of the WC–MgO composite in the NaCl solution is WO_3.

In order to further analyze the corrosion mechanism, the ICP is used to characterize the chemical composition of the 3.5% NaCl solution after the 60 day immersion test. According to Figure 10, the content of the Mg element is 12.22 mg/g and the content of the W element is 237.78 mg/g. It is obvious that the MgO phase is dissolved in the NaCl solution, while the WC matrix is not only oxidized but also dissolved in the NaCl solution.

3.3. Corrosion Mechanism

The surface corrosion micromorphology corroded in the 1 wt.% and 10 wt.% NaCl solutions is shown in Figure 11. The typical pitting corrosion characteristic is found for the WC–MgO composite in the NaCl solution. It is obvious that the pitting pits corroded in the 1 wt.% NaCl solution are bigger and in a large quantity compared with in the 10 wt.% NaCl solution. According to the Tafel and EIS results, as shown in Figures 2 and 3, the WC–MgO composite possesses the worst corrosion performance in the 1 wt.% NaCl solution. Meanwhile, the WC–MgO composite possesses better corrosion resistance in the 10 wt.% NaCl solution. Hence, the corrosion micromorphology further confirms the Tafel and EIS results.

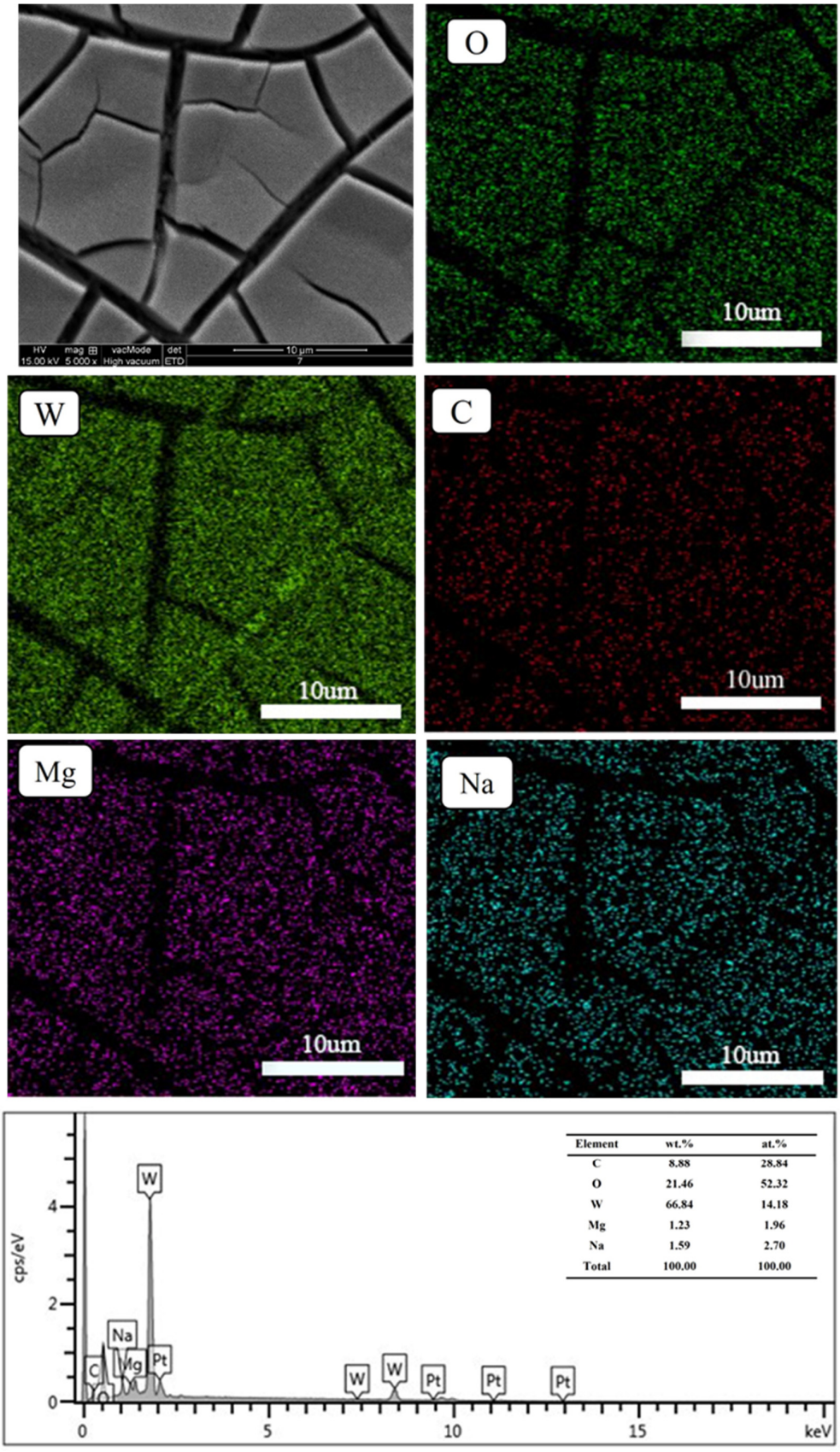

Figure 8. Mapping EDS of corrosion products on the surface of WC–MgO composite in 1 wt.% NaCl solution.

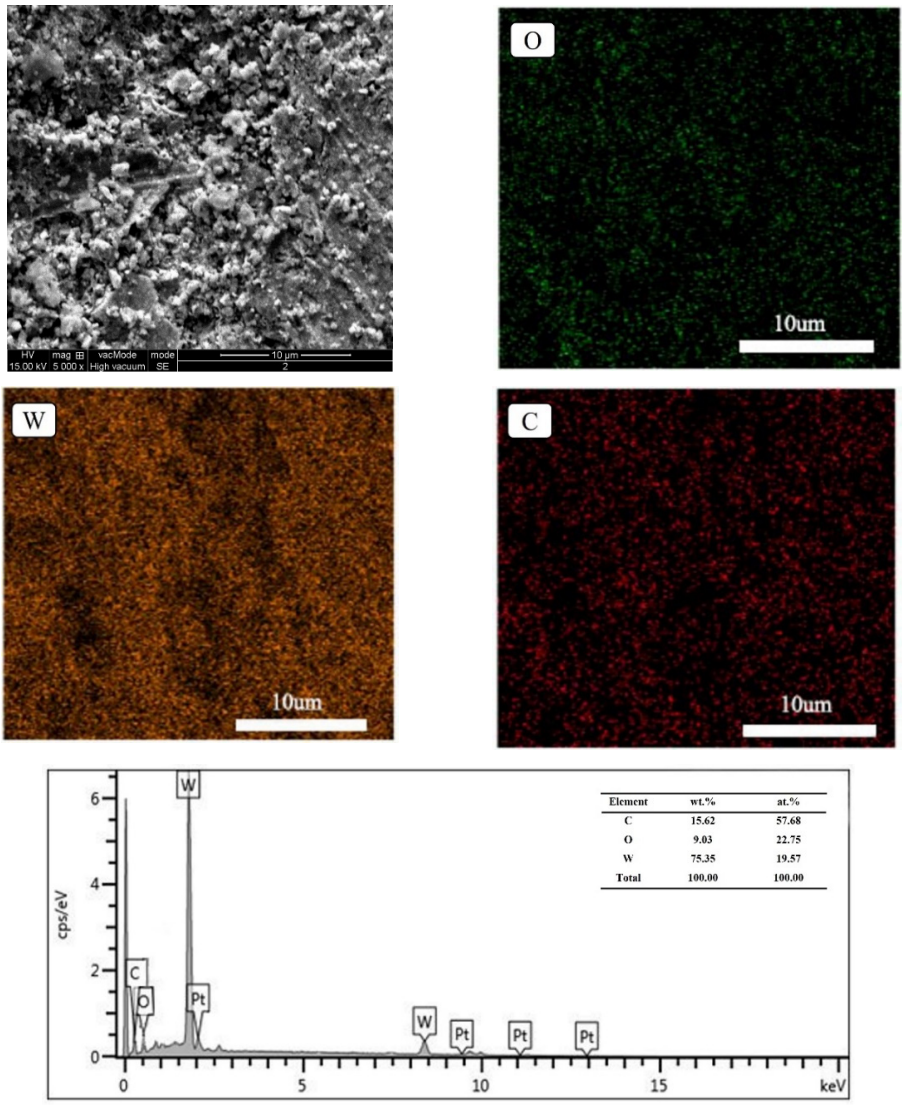

Figure 9. Mapping EDS of corrosion products on the surface of WC–MgO composite in 3.5 wt.% NaCl solution.

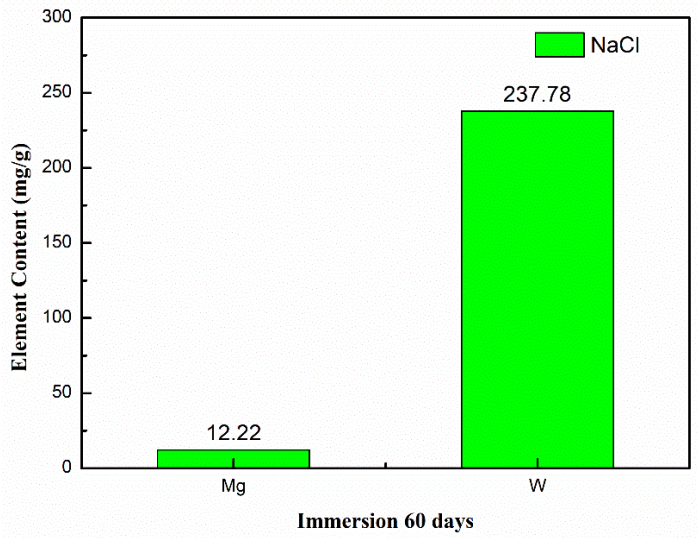

Figure 10. Content of Mg and W elements in 3.5% NaCl solution after soaking for 60 days.

As we all know, the electrode reaction mainly includes the following three processes: (1) the reactants are transferred from the inside to the interface; (2) the reactants react on the surface and produce reaction products; (3) the reaction products diffuse away from the interface reaction zone. It is seen that the electrode reaction includes several complicated processes, such as adsorption, charge transfer, pre-chemical reaction, post-chemical reaction, etc. [28]. Hence, for the WC–MgO composite, the main influence factors are attributed to the solution conductivity and concentration of the dissolved oxygen in the NaCl solution. The solution conductivity determines the charge transfer process, and the dissolved oxygen determines the cathodic oxygen absorption reaction.

When the Cl^- concentration is low, such as in the 0.1 wt.% NaCl solution, the content of the conductive ions (Na^+ and Cl^-) is very low. In this situation, poor conductivity becomes the main factor restricting the electrochemical reaction. Hamann et al. [29] pointed out that the linear relationship between conductivity and electrolyte concentration only holds in a dilute solution system. When the electrolyte concentration is high, the conductivity will remain stable. The main reason is attributed to a strong Coulomb force, which promotes positive and negative ions to form neutral particles. Hence, the solution conductivity hinders the process of charge transfer when the Cl^- concentration is extremely low. At this time, the charge transfer step becomes the reaction rate control step of the electrochemical reaction.

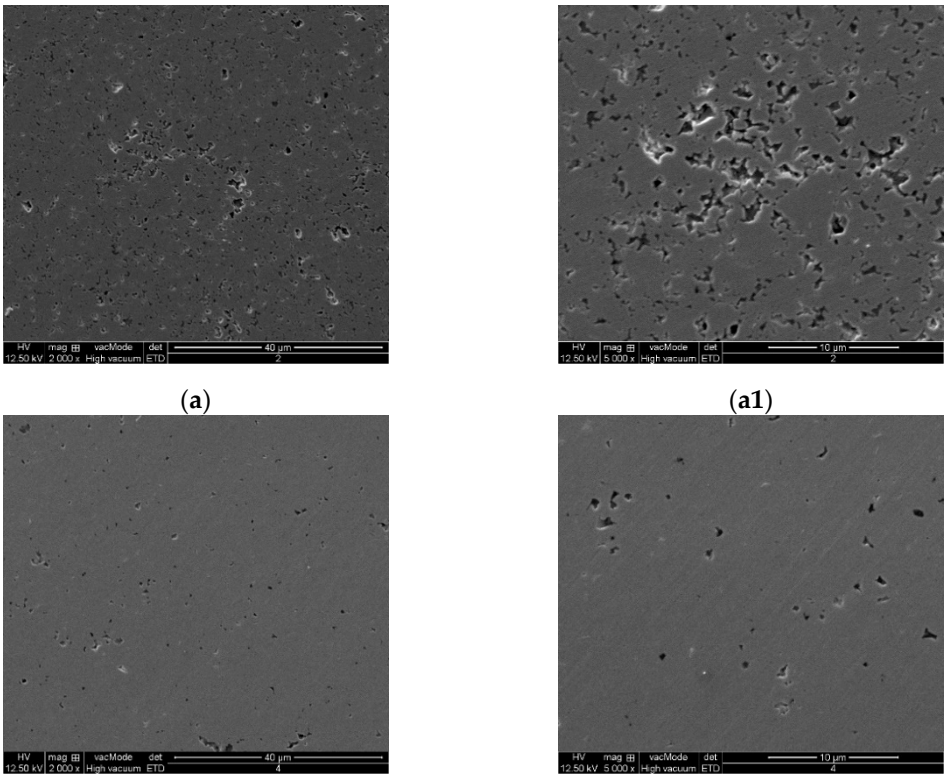

(**a**) (**a1**)

(**b**) (**b1**)

Figure 11. Corrosion morphology of WC–MgO composite in 1 wt.% NaCl (**a**,**a1**) and 10 wt.%NaCl (**b**,**b1**) solution.

According to XRD and mapping EDS, it is confirmed that the WC phase is oxidized to form a WO_3 film, as shown in Equation (1). The WO_3 film is also found in the WC–Co cemented carbide corroded by the NaCl solution [30]. The cathodic reaction is the reduction of dissolved oxygen, as shown in Equation (2) [31].

$$WC + 5H_2O \rightarrow WO_3 + CO_2 + 10H^+ + 10e^- \quad (1)$$

$$O_2 + 2H_2O + 4e^- \rightarrow 4OH^- \quad (2)$$

It is obvious that the concentration of dissolved oxygen possesses a significant influence on the electrochemical corrosion process. According to the relationship between dissolved oxygen and Cl^- concentration, as shown in Figure 4, the increase in Cl^- concentration causes a rapid decrease in the dissolved oxygen content. According to Figure 5, the corrosion current density decreases by about 96.3% and the total impedance increases by about 59.1% when the dissolved oxygen is removed from the NaCl solution. It further proves that the dissolved oxygen content has an important impact on the corrosion rate. Obviously, when the Cl^- concentration is 1 wt.%, the corrosion solution has good conductivity and a relatively high dissolved oxygen content. Therefore, the WC–MgO composite possesses the fastest corrosion rate in the 1 wt.% NaCl solution. Apparently, the content of dissolved oxygen decreases significantly when the Cl^- concentration reaches 10 wt.%, which inhibits the progress of the electrochemical cathodic reaction. This will inevitably decrease the corrosion rate of the WC–MgO composite.

According to the ICP result, as shown in Figure 10, it is inferred that the MgO phase and the WC phase are dissolved in the NaCl solution. Because of the poor conductivity of the MgO [32], the dissolution process of the MgO is a kind of chemical corrosion. As shown in Equation (3), the MgO phase can react with H_2O spontaneously to form porous $Mg(OH)_2$ [33,34]. Then, $Mg(OH)_2$ reacts with Cl^- to form $MgCl_2$, as shown in Equation (4) [35].

$$MgO + H_2O \rightarrow Mg(OH)_2 \quad (3)$$

$$Mg(OH)_2 + 2Cl^- \rightarrow MgCl_2 + 2OH^- \quad (4)$$

Rashad et al. [36,37] further point out that $Mg(OH)_2$ possesses a porous structure. Therefore, Cl^- can easily pass through the corrosion product layer and continuously react with $Mg(OH)_2$. The dissolution of the MgO phase provides the initial position for pitting corrosion. Banerjee et al. [35] also point out that pit generation can be attributed to the formation of $MgCl_2$. Meanwhile, the OH^- is generated in the process of the MgO dissolution, as shown in Equation (4), which increases the local PH value and forms the WC matrix in local alkaline. Previous studies point out that it is easy to dissolve the WC phase in an alkaline solution [24], as shown in Equation (5). The ICP result confirms the dissolution of the WC phase in the NaCl solution. Hence, the dissolution of the WC matrix is the major reason for pitting development inside.

$$WC + 14OH^- \rightarrow WO_4^{2-} + CO_3^{2-} + 7H_2O + 10e^- \quad (5)$$

The schematic diagram of the corrosion mechanism is shown in Figure 12. The corrosion destruction is attributed to the dissolution of MgO, which is the initial source of pitting. The oxidation of WC contributes to the formation of the protective passivation film, which inhibits uniform corrosion. It is seen that the alkaline environment caused by the dissolution of MgO promotes the destruction of the inner WC matrix. Due to the extremely small area of pitting, the current density is extremely high. This is the so-called "large anode and small cathode" area, which induces a fast corrosion rate [38]. According to Faradic law [39], the amount of charge transfer is directly proportional to material loss. In a low-concentration NaCl solution, poor conductivity inhibits the charge transfer process. However, in high-concentration solutions, the cathodic oxygen absorption reaction is inhibited, thereby increasing the corrosion resistance. Hence, in the 1 wt.% NaCl solution, high conductivity and sufficient dissolved oxygen promote the electrochemical corrosion process, resulting in the worst corrosion performance of the WC–MgO composite.

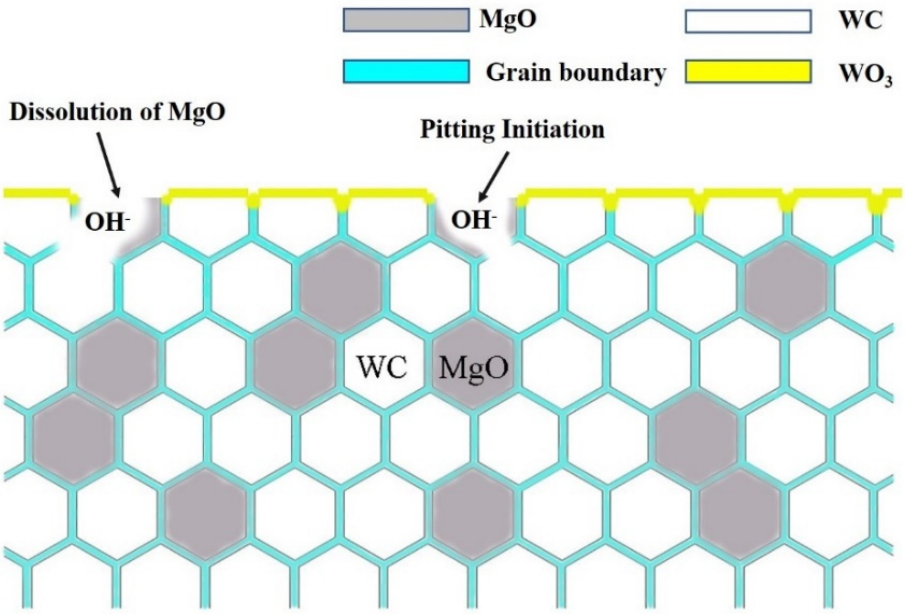

Figure 12. Schematic diagram of corrosion mechanism of WC–MgO composite in NaCl solution.

4. Conclusions

In this paper, the corrosion behavior of the WC–MgO composite in different concentration NaCl solutions was studied. The corrosion mechanism of the WC–MgO composite in a neutral NaCl solution was clarified. The following conclusions were obtained:

(1) The corrosion resistance of WC–MgO composite decreased first, then increased with the increase in Cl^- concentration, which was attributed to the solution conductivity and dissolved oxygen content. The solution conductivity determined the charge transfer process, and the dissolved oxygen determined the cathodic oxygen absorption reaction.

(2) The corrosion destruction was due to the oxidation of WC and dissolution of MgO. The main corrosion product was WO_3. The formation of the WO_3 corrosion layer on the surface hindered the general corrosion to protect the inner material.

(3) The corrosion characteristic had typical pitting corrosion. The dissolution of MgO induced the initiation of pitting. The local alkaline caused by the MgO dissolution promoted the dissolution of the WC matrix, which led to the expansion of pitting.

Author Contributions: The following contributions were made by each co-author. Conceptualization, B.F.; methodology, B.F. and T.Q.; resources, B.F. and Y.Z.; data curation, B.F. and J.W.; writing—original draft preparation, B.F.; writing—review and editing, B.F., T.Q., Y.Z. and J.W. All authors have read and agreed to the published version of the manuscript.

Funding: This research was funded by The Natural Science Foundation of the Jiangsu Higher Education Institutions of China (No. 23KJB430037), Scientific Research Project of Wuxi Institute of Technology (No. BT2023-03).

Data Availability Statement: The data, supporting results, and reported results in general can be provided by the author upon request.

Acknowledgments: We greatly thank the grants and funds provided to carry out this work.

Conflicts of Interest: The authors declare no conflicts of interest.

References

1. Tang, X.; Wang, Z.; Huang, L.; Wang, X.; Chang, T.; Huang, P.; Zhu, Z. Preparation, properties and microstructure of high hardness WC–Co cemented carbide tool materials for ultra-precision machining. *Int. J. Refract. Met. Hard Mater.* **2023**, *116*, 106356. [CrossRef]
2. Li, X.; Wang, L.; Liu, Y.; Ye, J. Enhanced high temperature mechanical properties of WC–Co cemented carbides by VC addition. *Int. J. Refract. Met. Hard Mater.* **2023**, *116*, 106355. [CrossRef]
3. Zhou, B.; Wang, H.; Lu, H.; Liu, X.; Liu, C.; Wen, X.; Fan, C.; Song, X. WC–Co–TiNbZr composite with simultaneously high hardness and fracture toughness. *Int. J. Refract. Met. Hard Mater.* **2023**, *116*, 106332. [CrossRef]
4. Nino, A.; Takahashi, H.; Sekine, T.; Sugiyama, S. Effects of Si_3N_4 addition on the microstructure and mechanical properties of binderless tungsten carbides. *Int. J. Refract. Met. Hard Mater.* **2023**, *114*, 106267. [CrossRef]
5. Yang, M.; Han, B.; Guo, Z.; Luo, X.; Wang, T. Pressureless sintering of WC-TaC binderless carbide. *Ceram. Int.* **2020**, *46 Pt A*, 28814–28820. [CrossRef]
6. Ozawa, A.; Morimoto, S.; Hatayama, H.; Anzai, Y. Energy–materials nexus of electrified vehicle penetration in Japan: A study on energy transition and cobalt flow. *Energy* **2023**, *277*, 127698. [CrossRef]
7. Wu, J.; Zhang, Z.; Wang, H.; Wang, C.; Hou, Z.; Wu, D.; Ouyang, X. High–pressure synthesis of tungsten carbide–cubic boron nitride (WC–cBN) composites: Effect of cBN particle size and volume fraction on their microstructure and properties. *Int. J. Refract. Met. Hard Mater.* **2023**, *110*, 106037. [CrossRef]
8. Liang, Z.; Liu, X.; Zhao, Z.; Lu, H.; Wang, H.; Liu, C.; Wang, M.; Song, X. Enhancing hardness and toughness of WC simultaneously by dispersed ZrO2. *Mater. Sci. Eng. A* **2023**, *870*, 144905. [CrossRef]
9. Hui, J.; Han, B.; Weiwei, D.; Zhu, S. High-temperature oxidation behaviour of vacuum hot-pressed WC–15 wt% Al_2O_3 composites. *Ceram. Int.* **2022**, *48*, 12184–12192. [CrossRef]
10. Radajewski, M.; Schimpf, C.; Krüger, L. Study of processing routes for WC–MgO composites with varying MgO contents consolidated by FAST/SPS. *J. Eur. Ceram. Soc.* **2017**, *37*, 2031–2037. [CrossRef]
11. Katiyar, P.K.; Randhawa, N.S. Corrosion behavior of WC–Co tool bits in simulated (concrete, soil, and mine) solutions with and without chloride additions. *Int. J. Refract. Met. Hard Mater.* **2019**, *85*, 105062. [CrossRef]
12. Herrmann, M.; Klemm, H. 2.15—Corrosion of Ceramic Materials. In *Comprehensive Hard Materials*; Sarin, V.K., Ed.; Elsevier: Oxford, UK, 2014; pp. 413–446.
13. Cardoso, J.P.; Puga, J.; Rocha, A.F.; Fernandes, C.M.; Senos, A.M. WC—(Cu:AISI304) composites processed from high energy ball milled powders. *Int. J. Refract. Met. Hard Mater.* **2019**, *84*, 104990. [CrossRef]
14. Liang, F.; Du, J.; Su, G.; Zhang, P.; Zhang, C. Investigating the effect of Al, Mo or Mn addition to CoCrFeNi entropy alloys on the interface binding properties of WC/HEA cemented carbides. *Mater. Today Commun.* **2023**, *35*, 105891. [CrossRef]
15. Fazili, A.; Derakhshandeh, M.R.; Nejadshamsi, S.; Nikzad, L.; Razavi, M.; Ghasali, E. Improved electrochemical and mechanical performance of WC–Co cemented carbide by replacing a part of Co with Al_2O_3. *J. Alloys Compd.* **2020**, *823*, 153857. [CrossRef]
16. Yang, X.-H.; Wang, K.-F.; Zhang, G.-H.; Chou, K.-C. WC–VC/Cr_3C_2 composite powders prepared by a carbothermic reduction-carburization process. *Int. J. Refract. Met. Hard Mater.* **2022**, *109*, 105982. [CrossRef]
17. Tang, W.; Zhang, L.; Chen, Y.; Zhang, H.; Zhou, L. Corrosion and strength degradation behaviors of binderless WC material and WC–Co hardmetal in alkaline solution: A comparative investigation. *Int. J. Refract. Met. Hard Mater.* **2017**, *68*, 1–8. [CrossRef]
18. Wang, W.; Wang, J.; Zhang, M.; Lan, H.; Zhao, S.; Liang, C.; Xu, F.; Shao, L.; Zhu, D.; Dai, S.; et al. SiC_w strengthened WC-Y_2O_3 composite and its electrochemical corrosion in aggressive medium. *Int. J. Refract. Met. Hard Mater.* **2024**, *119*, 106517. [CrossRef]
19. Han, B.; Zhu, S.; Dong, W.; Bai, Y.; Ding, H.; Luo, Y.; Di, P. Improved electrochemical corrosion resistance of hot-press sintered WC-Al_2O_3 composites with added TiC in alkaline solutions. *Ceram. Int.* **2021**, *47*, 32168–32178. [CrossRef]
20. Ma, J.; Zhu, S.; Ouyang, C. Two-step hot-pressing sintering of nanocomposite WC–MgO compacts. *J. Eur. Ceram. Soc.* **2011**, *31*, 1927–1935. [CrossRef]
21. Ouyang, C.; Zhu, S.; Qu, H. VC and Cr_3C_2 doped WC–MgO compacts prepared by hot-pressing sintering. *Mater. Des.* **2012**, *40*, 550–555. [CrossRef]
22. Fan, B.; Zhu, S.; Ding, H.; Bai, Y.; Luo, Y.; Di, P. Influence of MgO whisker addition on microstructures and mechanical properties of WC–MgO composite. *Mater. Chem. Phys.* **2019**, *238*, 121907. [CrossRef]
23. Ouyang, C.; Zhu, S.; Li, D.Y. Corrosion and corrosive wear behavior of WC–MgO composites with and without grain-growth inhibitors. *J. Alloys Compd.* **2014**, *615*, 146–155. [CrossRef]
24. Fan, B.; Zhu, S.; Dong, W.; Ding, H.; Bai, Y.; Luo, Y.; Di, P. The study of corrosion behavior of WC–MgO composite in H_2SO_4 and NaOH solution. *Ceram. Int.* **2021**, *47*, 1364–1372. [CrossRef]
25. Fan, B.; Zhu, S.; Dong, W.; Ding, H.; Bai, Y.; Luo, Y.; Di, P. Comparative study on corrosion behavior of WC–MgO composite and WC-6Co cemented carbide in NaCl solution. *Ceram. Int.* **2021**, *47*, 7106–7116. [CrossRef]
26. Wang, Z.; Feng, Z.; Fan, X.-H.; Zhang, L. Pseudo-passivation mechanism of CoCrFeNiMo0.01 high-entropy alloy in H_2S–containing acid solutions. *Corros. Sci.* **2021**, *179*, 109146. [CrossRef]
27. Raja, K.; Jones, D. Effects of dissolved oxygen on passive behavior of stainless alloys. *Corros. Sci.* **2006**, *48*, 1623–1638. [CrossRef]
28. Exner, K.S. *Elementary Reaction Steps in Electrocatalysis: Theory Meets Experiment*; Elsevier: Oxford, UK, 2024; pp. 65–92.
29. Arrigan, D. Electrochemistry. *Chromatographia* **2010**, *71*, 351. [CrossRef]

30. Ghosh, G.; Sidpara, A.; Bandyopadhyay, P. Understanding the role of surface roughness on the tribological performance and corrosion resistance of WC–Co coating. *Surf. Coat. Technol.* **2019**, *378*, 125080. [CrossRef]
31. da Silva, F.; Cinca, N.; Dosta, S.; Cano, I.; Couto, M.; Guilemany, J.; Benedetti, A. Corrosion behavior of WC–Co coatings deposited by cold gas spray onto AA 7075-T6. *Corros. Sci.* **2018**, *136*, 231–243. [CrossRef]
32. Shand, M.A. *The Chemistry and Technology of Magnesia*; John Wiley & Sons, Inc.: Hoboken, NJ, USA, 2006.
33. Luo, Y.; Sun, Y.; Lv, J.; Wang, X.; Li, J.; Wang, F. Transition of interface oxide layer from porous $Mg(OH)_2$ to dense MgO induced by polyaniline and corrosion resistance of Mg alloy therefrom. *Appl. Surf. Sci.* **2015**, *328*, 247–254. [CrossRef]
34. Song, G.; Atrens, A.; Wu, X.; Zhang, B. Corrosion behaviour of AZ21, AZ501 and AZ91 in sodium chloride. *Corros. Sci.* **1998**, *40*, 1769–1791. [CrossRef]
35. Banerjee, S.; Poria, S.; Sutradhar, G.; Sahoo, P. Corrosion behavior of AZ31-WC nano-composites. *J. Magnes. Alloys* **2019**, *7*, 681–695. [CrossRef]
36. Rashad, M.; Pan, F.; Asif, M.; Chen, X. Corrosion behavior of magnesium–graphene composites in sodium chloride solutions. *J. Magnes. Alloys* **2017**, *5*, 271–276. [CrossRef]
37. Rashad, M.; Pan, F.; Yu, Z.; Asif, M.; Lin, H.; Pan, R. Investigation on microstructural, mechanical and electrochemical properties of aluminum composites reinforced with graphene nanoplatelets. *Prog. Nat. Sci.* **2015**, *25*, 460–470. [CrossRef]
38. Zhang, L.; Yan, H.; Zou, Y.; Yu, B.; Hu, Z. Effect of adding rare-earth cerium on the microstructure and acid rain corrosion resistance of the ADC12 alloy. *Int. J. Mater. Res.* **2021**, *112*, 241–249. [CrossRef]
39. Jia, H.; Feng, X.; Yang, Y. Microstructure and corrosion resistance of directionally solidified Mg-2 wt.% Zn alloy. *Corros. Sci.* **2017**, *120*, 75–81. [CrossRef]